Light-Off Location and Front Diffusion in a Catalytic Monolith Reactor

Karthik Ramanathan and Ashok Gopinath
India Science Lab, General Motors Research and Development Division, Creator Building, International Technology Park, Bangalore, Karnataka 560066, India

DOI 10.1002/aic.11517
Published online May 15, 2008 in Wiley InterScience (www.interscience.wiley.com).

A one-dimensional solid–gas model has been used to study the light-off behavior in a reactor system. Techniques from nonlinear analysis are applied to first arrive at an analytical expression to estimate the light-off location in the reactor. The model is then extended to estimate the thickening of the light-off front in the vicinity of the light-off location due to heat diffusion effects in the solid substrate. Both these results are expressed in terms of all the important operating and design variables of the monolith reactor and also the reaction specific variables such as the kinetic parameters and heats of reaction. A specific case of a three-way catalyst (TWC) is numerically treated in detail to illustrate the application of this work. Finally, we focus on using the insight obtained from this study to suggest design guidelines to optimize the performance of automotive catalytic monolith reactors. *AIChE J,* 54: 1860–1873, 2008
Keywords: catalytic monolith reactor, light-off location, spread of the light-off front, exhaust gas aftertreatment, automobile emissions

Introduction and Literature Review

Catalytic monoliths are one of the most widely used forms of catalytic reactors. One of the major advantages of such reactors over traditional packed bed reactors is the lower pressure drops that they afford for the high flow rates that are encountered in many industrial applications. One of the most common applications of a monolith reactor is in the control of automobile emissions. In the automobile industry, monolith reactors are used in a three-way catalyst (TWC) to reduce the emissions of CO, hydrocarbons, and NO_x, as an oxidation catalyst in a DOC (diesel oxidation catalyst) for diesel engine applications, and in LNT (Lean NO_x Trap) and SCR (selective catalytic reduction) applications for reducing NO_x emissions. Apart from these uses, monolith reactors find application in catalytic combustion, catalytic oxidation of VOCs, selective catalytic removal of NO_x from power plant and furnace exhausts, and catalytic partial oxidation of hydrocarbons. They are also currently being evaluated for carrying out liquid phase reactions as well as gas–liquid reactions. Other emerging applications include hydrogen generation in fuel cells and steam reforming of hydrocarbons.

The monolith reactor is a unitary structure usually made of a ceramic material and consisting of a large number of thin-walled, narrow, parallel flow channels that makes up the substrate. The catalyst is deposited on the walls of the narrow channels either as a thin layer or as a porous washcoat which is supported on the monolith substrate. The gas that enters the reactor is transported by convection and diffusion in parallel flow streams through these narrow channels and reactions occur on the active catalytic surfaces present in the washcoat. Since there is a complex coupling of the physical and chemical processes in the monolith, improvements in the design of such reactors require a comprehensive understanding of the influence of various design and operating variables on the performance of the monolith. The various review articles[1–7] summarize the recent progress in catalytic monolith reactors.

Correspondence concerning this article should be addressed to K. Ramanathan at karthik.ramanathan@gm.com.

Mathematical modeling and simulation are useful in identifying the optimal designs and reducing the amount of experimentation needed to achieve this goal. Mathematical models of varying degrees of complexity (in terms of the geometric dimensionality of the model, flow modeling, washcoat diffusion modeling, and chemical kinetics modeling) have been in use over the last 2–3 decades.[8–26] In particular, the one-dimensional two-phase (gas–solid) model[26,27] which differentiates between the gas and solid phase concentrations and temperatures has been found to describe these processes in a monolith reactor quite satisfactorily.[28,29]

The ability to determine the light-off location and the thickness of the light-off front in a monolith reactor is particularly desirable in a TWC to be able to predict its performance and minimize cold-start emissions. The performance of a TWC depends significantly on the operating conditions (inlet gas flow rate, temperature, and species concentrations) and design parameters such as amount and distribution of catalyst, cell density, channel length, etc. In this study, mathematical techniques from nonlinear analysis have been applied to a suitable reactor model to obtain an analytical expression (which includes the effect of all operating and design parameters) that predicts the location of light-off in a TWC converter. This result can be used to predict light-off location and light-off time (indirectly) in a TWC, and also to find the minimum inlet temperature, the minimum channel length, and the minimum amount of catalyst required to achieve this condition. In addition, an analysis of the mechanics of heat diffusion in the light-off front can be used to determine the front thickness and to understand the extent to which the light-off is localized or homogenized. The model developed here could therefore be used to establish the optimal operating and design parameters that would help achieve localized near-inlet light-off that would maximize the reduction in cold-start emissions. Although the specific case of a TWC has been considered in this study as an illustrative numerical example, the underlying analysis is general and can be applied to other flow-through monolith based catalytic reactor systems.

Previous studies in the literature[30–35] on light-off behavior have been worked out for simpler cases of a single reaction (and/or first order kinetics) and/or have been largely restricted to the prediction of light-off with the assumption of negligible heat conduction in the substrate. A more recent study[35] examines a design that uses preheating to ensure stable and early leading-edge ignition based on the extension of an earlier study.[34] In this work, the light-off location and diffusional spread of the reaction front are determined for the general case of multiple reactions and complex kinetics in the presence of finite substrate heat conduction and the effect of different parameters on this behavior is illustrated through a numerical example. Finally, we discuss how the results from this study can be used to arrive at better and more generalized design guidelines for tuning the performance of catalytic monolithic reactors.

Mathematical Model

The governing equations in our one-dimensional mathematical model describing the mass and energy balances of the solid phase and the gas phase in a catalytic monolith through-flow reactor are given by[26]:

$$(f_{sb}\rho_{sb}C_{p,sb} + f_{wc}\rho_{wc}C_{p,wc})\frac{\partial T_s}{\partial t} = f_{sb}\lambda_{sb}\frac{\partial^2 T_s}{\partial z^2} + hS(T_g - T_s) - \sum_{j=1}^{n\text{Rct}} a_j(z)(\Delta H)_j R_j \quad (1)$$

$$\frac{w}{A}C_{p,g}\frac{\partial T_g}{\partial z} = hS(T_s - T_g) \quad (2)$$

$$\frac{w}{A}\frac{\partial x_{g,i}}{\partial z} = -k_{m,i}S(x_{g,i} - x_{s,i}) = \sum_{j=1}^{n\text{Rct}} a_j(z)s_{ij}R_j \qquad i = 1, 2, ..., n\text{Species}. \quad (3)$$

Equations 1 and 2 represent the energy balance for the solid and gas phase, respectively and Eq. 3 represents the solid and gas phase mass balances. Here, "T" and "x" represent the gas temperature and species mole fractions, while the subscripts "s" and "g" refer to the solid and the gas phase, respectively. In the above equations, "nRct" represents the number of reactions and "nSpecies" represents the number of reacting species. The subscripts "wc" and "sb" refer to the washcoat and the substrate, respectively. The subscripts i and j represent the ith species and the jth reaction, respectively, and the elements of the matrix s_{ij} represent the corresponding stoichiometric coefficients. The R_j's represent the reaction rate expressions for the different reactions and are dependent on the solid substrate temperature and various gas species concentrations. All the other variables have their usual meanings and are explained in the nomenclature section. The boundary and initial conditions are given by

$$\begin{aligned} T_g &= T_{g,in}(t) \quad \text{at } z = 0 \\ x_{g,i} &= x_{g,in,i}(t) \quad \text{at } z = 0 \\ \frac{\partial T_s}{\partial z} &= 0 \quad \text{at } z = 0, L \\ T_s(z) &= T_{s,init} \quad \text{at } t = 0. \end{aligned} \quad (4)$$

The mass ($k_{m,i}$) and heat transfer (h) coefficients inside the reactor channels are expressed in terms of the corresponding Sherwood and Nusselt numbers as

$$\begin{aligned} k_{m,i} &= \frac{Sh_{D_h}}{D_h}(cD_{i,m}) \\ h &= \frac{Nu_{D_h}}{D_h}\lambda g \end{aligned} \quad (5)$$

where the thermal conductivity of the gas (λ_g) and the mass diffusivity ($D_{i,m}$) are given by[36,37]:

$$\begin{aligned} \lambda_g(T_g) &= 2.66 \times 10^{-4}\, T_g^{0.805} \quad [\text{W/m} - \text{K}] \\ cD_{i,m} &= \frac{1.01325 \times 10^{-2}\, T_g^{0.75}\sqrt{\frac{1}{M_i} + \frac{1}{M_{N_2}}}}{R_g\left[\sqrt[3]{\sum i} + \sqrt[3]{\sum_{N_2}}\right]^2} \quad [\text{mol/m}^2 s] \end{aligned} \quad (6)$$

where M_i represents the molecular weight of the ith species and Σ_i represents the diffusion volume of the species.[37] In

Eq. 5, Nu_{D_h} represents the Nusselt number and Sh_{D_h} represents the Sherwood number, both based on D_h which represents the channel hydraulic diameter. More details about the model can be found in the literature.[26,27]

Light-Off Location

It is important to first define the concept of light-off in this study. It may be noted that there are many alternate but similar definitions of light-off in the literature[38–43]—one of the commonly used ones refers to light-off as the temperature condition required to achieve 50% conversion although we do not use this definition in the current work. Light-off in this work assumes or implies that a plot of the steady-state (bifurcation) diagram of solid temperature (or gas phase exit conversion or temperature) as a function of the inlet gas temperature exhibits a generalized S-shaped behavior in which the ignition or light-off point is represented by the normal limit point in the feasible region.

Figure 1 is a schematic of such an S-shaped curve which is also known as the temperature ignition-extinction curve.[44,45] As shown in this figure, as we increase the inlet gas temperature, the solid temperature/conversion behavior could progress along one of the (solid or dashed) curves. When the system parameters are such that it does not exhibit multiple solutions (i.e., the system parameters are not in the region of multiple solutions), the behavior is depicted by the dashed curve. On the other hand, when multiple solutions are favored, the system follows the solid curve. The light-off point then represents the normal limit point in such a bifurcation diagram at which such a branch jump condition is possible and the corresponding inlet gas temperature represents the minimum temperature required to achieve this condition. So in theory, as we approach the light-off point in a reactor system, a small increase in the inlet temperature leads to a large increase in the solid temperature (and conversion) to the higher temperature branch of the system indicative of a dramatic step change in the state variables across an infinitesimally thin reaction front. In simple terms, light-off essentially represents the condition where enough heat has been generated in the reactor system for the reaction(s) to "spark off". Once light-off has been achieved, reactor operation changes to the high temperature branch in the bifurcation diagram (cf. Figure 1) and the reactor can be said to have transitioned from a kinetically controlled regime to a regime that is usually mass transfer controlled. Throughout this study we assume that the system parameters are in the regime that support light-off as represented by the solid curve in the bifurcation diagram of Figure 1.

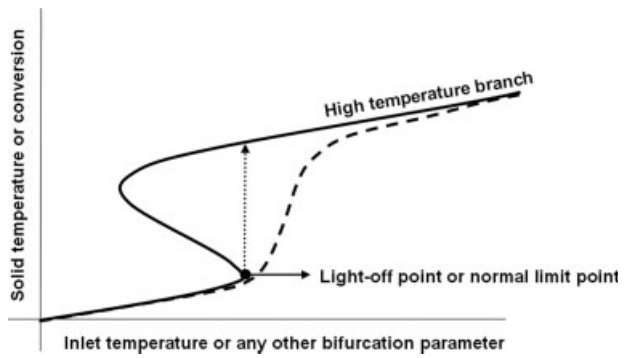

Figure 1. Schematic of the variation of the solid temperature or species conversion with the inlet temperature of the gas.

In a typical reactor system, there are in general two possibilities as shown by the solid and dashed curves.

In this section, the mathematical model presented earlier will be used to derive an analytical expression for the light-off location in the catalytic reactor. The following assumptions have been made in this process:

(1) The reactor is under steady state operating conditions. Later in this section, as well as in concluding discussion, we explain the impact of this assumption on the behavior of transient reactor systems.

(2) The catalyst loading/activity is uniform along the length of the reactor monolith, i.e., $a_j(z) = a_j = \text{constant}$.

(3) Solid conduction (or heat diffusion) in the monolith substrate is assumed to be negligible ($\lambda_{sb} \approx 0$) which is satisfactory for predicting the location of the light-off front. However in the next section we relax this assumption to find the spread of the light-off front at this location. (We discuss the limiting case of infinite substrate conduction and its effects in an Appendix).

(4) The internal laminar channel flow Nusselt and Sherwood numbers are assumed constant at their fully developed values and calculated at a suitable reference temperature. This is justified due to the typically highly laminar nature of the flow with small flow Reynolds numbers and correspondingly small entrance lengths.

(5) The consumption of the reactant species before the light-off location is assumed to be negligible. Since the primary interest is in predicting the light-off behavior, we assume that the species concentrations just before the light-off location are essentially equal to the inlet concentrations (since negligible or very little reaction takes place) in this kinetically controlled regime of the reactor. In other words, the species mass transfer between the surface and the bulk is relatively very rapid in the section of the reactor upstream of the light-off location thereby making the process reaction-rate-limited (kinetics limited) and the surface and bulk species concentrations essentially equal ($c_{s,i} \approx c_{g,i}$) in this region.

Most of the above assumptions are well justified and fairly common in the literature although a detailed rationalization of some of them will be provided later. With the above assumptions, the solid and gas phase energy balances can be written as

$$hS(T_g - T_s) - \sum_{j=1}^{n\text{Rct}} a_j(\Delta H)_j R_j(x_{g,in}, T_s) = 0 \tag{7}$$

$$\frac{w}{A} C_{p,g} \frac{\partial T_g}{\partial z} = hS(T_s - T_g). \tag{8}$$

The light-off point (normal limit point) for a system described by the above set of equations is obtained by differentiating Eq. 7 partially with respect to T_s and setting it equal to zero since this is a necessary condition for the singularity at the limit-point[44,45] (see also Figure 1) to get,

$$-hS-\sum_{j=1}^{n\mathrm{Rct}} a_j(\Delta H)_j \frac{\partial}{\partial T_s}\left(R_j(x_{g,in},T_s)\right)=0. \tag{9}$$

The reactor lights-off when the solid temperature reaches a critical value called the light-off temperature ($T_{s,lo}$) obtained by solving the above equation for T_s.

To determine the light-off location, we combine Eqs. 7 and 8 and use the result for $\partial T_g/\partial T_s$ from Eq. 7 to obtain:

$$\frac{w}{A}C_{p,g}\frac{dT_s}{dz}=\frac{\left(-\sum_{j=1}^{n\mathrm{Rct}} a_j(\Delta H)_j R_j(x_{g,in},T_s)\right)}{\left(1+\dfrac{\sum_{j=1}^{n\mathrm{Rct}} a_j(\Delta H)_j \dfrac{dR_j(x_{g,in},T_s)}{dT_s}}{hS}\right)} \tag{10}$$

which is now integrated from $z = 0$ to $z = z_{lo}$, where z_{lo} represents the location of light-off. The corresponding solid temperature varies from $T_{s,in}$ to $T_{s,lo}$, where $T_{s,in}$ represents the solid temperature corresponding to the inlet gas temperature, $T_{g,in}$, and is obtained by solving $T_{s,in}$ in Eq. 7 at the inlet according to

$$hS(T_{g,in}-T_{s,in})-\sum_{j=1}^{n\mathrm{Rct}} a_j(\Delta H)_j R_j(x_{g,in},T_{s,in})=0.$$

The above results can be combined to obtain the following result for the light-off location

$$z_{lo}=\frac{wC_{p,g}}{hSA}\ln\left(\frac{\sum_{j=1}^{n\mathrm{Rct}} a_j(\Delta H)_j R_j(x_{g,in},T_{s,in})}{\sum_{j=1}^{n\mathrm{Rct}} a_j(\Delta H)_j R_j(x_{g,in},T_{s,lo})}\right)+\frac{wC_{p,g}}{A}\int_{T_{s,in}}^{T_{s,lo}}\frac{dT_s}{\sum_{j=1}^{n\mathrm{Rct}} a_j(-\Delta H)_j R_j(x_{g,in},T_s)}. \tag{11}$$

Equation 11 gives the location of light-off and its dependence on the various operating and design parameters in a reactor system. If $z_{lo} > L$, then there is of course no light-off in that length of the reactor. If z_{lo} satisfies a suitable defined criterion, say $z_{lo} < 0.05L$, or $z_{lo} \leq 10^{-3}$ m, then the light-off can be said to be close to the inlet which is a desirable condition[32] to maximize species conversion. This condition can be achieved for a given monolith operating at a given flow rate by choosing the right catalyst loading (a_j) and/or having the appropriate inlet gas temperature ($T_{g,in}$). The above expression provides a direct analytical result, for instance, to determine the minimum amount of catalyst, or the minimum channel length for a given inlet gas temperature, that is required to achieve light-off at a certain location within the reactor.

We now provide a more detailed discussion of the assumptions made earlier and the light-off behavior. At steady state, the length of the reactor in the light-off region is given by $L - z_{lo}$, i.e., the section of the reactor from z_{lo} to L is on the high temperature branch of the bifurcation diagram (cf. Figure 1). If transient operation of the reactor is analyzed, it can be argued that the first location (in time) to light-off would be z_{lo} and the heat thereby generated subsequently lights-off the remainder of the reactor. This is because, substrate heat diffusion effects are negligible on the scale of the reactor length and hence to have a steady state light-off at z_{lo}, the light-off should have occurred first (in time) at z_{lo}. The heat generated due to the reactions in the solid phase is transferred to the gas phase which in turn transfers the heat back to the solid phase at locations ($z > z_{lo}$) downstream of the light-off location, thereby heating up and aiding the light-off in the rest of the reactor (from z_{lo} to L). At steady state, the entire section of the reactor with $z > z_{lo}$ is in the high temperature light-off regime (or in the regime where it is not kinetically controlled). Hence, Eq. 11 can indeed also be used under transient operating conditions with time-varying inlet gas temperature to estimate the light-off location in the monolith channel. It should also be pointed out that the extent of species conversion in the monolith reactor would depend on the ignited length ($L - z_{lo}$) of the monolith and hence a lower value of z_{lo} would help maximize the conversion efficiency.

The second assumption can be justified by noting that in most practical and industrial applications the catalyst is uniformly coated along the length of the monolith channels. Even in cases where the catalyst loading is zonal in nature and the resulting catalyst activity is nonuniform, it is usually designed to vary discretely in zonal sections in such a way that there is constant activity within each zone. Usually a higher catalytic activity is preferred in the zone near the inlet so as to achieve near-inlet light-off especially to reduce cold-start emissions.[32] To achieve this condition, Eq. 7 should have the right set of parameters (such as surface area, catalyst loading, inlet gas temperature, etc.) to be able to exhibit multiple solutions at the inlet and the resulting solid temperature should be able to transition to the higher temperature branch of the bifurcation system (cf. Figure 1). It can be shown that this behavior is obtained when the following condition is satisfied

$$\frac{\sum_{j=1}^{n\mathrm{Rct}} a_j(-\Delta H)_j R_j(x_{g,in},T_{s,lo})}{hS(T_{s,lo}-T_{g,in})}\geq 1 \tag{12}$$

where $T_{s,lo}$ is given by Eq. 9. Equation 12 follows from the fact that at a given inlet gas temperature, for multiple solutions to exist, the solid temperature that satisfies Eq. 7 should be greater than the light-off temperature and be on the high temperature branch. In other words, Eq. 12 expresses the requirement that at the light-off temperature the heat generated at the inlet should be greater than the heat removed to sustain this condition. When the above criterion is satisfied, a near-inlet light-off is achieved in the reactor. The minimum amount of catalyst required for such a near-inlet light-off condition can be obtained by solving Eq. 12, or by solving for the catalyst activity a_j using a suitable inlet proximity criterion such as $z_{lo} < 0.05L$ or, say, $z_{lo} \leq 10^{-3}$ m in Eq. 11. Note that Eq. 12 can be used even for a nonuniform catalyst distribution i.e., even if only the inlet catalytic activity satisfies Eq. 12 with $a_j = a_j(z = 0)$ (which could be different from the interior loading conditions) a near-inlet light-off can be achieved.

When solid conduction is included in the model, the light-off front is smeared in z and hence the z_{lo} predicted with Eq. 11 would give a conservative estimate of the length of the channel that is in the light-off region. A transient simulation with varying gas concentrations and with solid conduction included would increase the time required for light-off, as

the heat generated in the solid diffuses along the substrate wall and is not localized.

Spread of the Light-Off Front

It is also useful to extend our analysis in the above framework to examine the nature and spread of the light-off front due to substrate heat diffusion in the vicinity of the light-off location. Ideally it is assumed that the light-off bifurcation behavior follows an S-shaped curve (noted earlier as in Figure 1) with the light-off location being the limit point along the channel length at which the state variables (such as solid temperature or conversion factor) exhibit a dramatic step change in their conditions. This step change is representative, ideally, of a steep transition across a sharp front in the reaction conditions from a kinetically controlled regime to a mass-controlled regime over an infinitesimally thin light-off zone. However, in reality, the light-off zone is of finite thickness due to heat diffusion effects which were assumed negligible for predicting the light-off location, but can now be included to examine their role in influencing the physical extent of the light-off zone.

Assuming constant inlet species concentrations as before, the quasi-steady state approximation can be made as argued in the previous section to arrive at the following form of the solid phase energy balance in Eq. 1.

$$0 \approx f_{\mathrm{sb}}\lambda_{\mathrm{sb}}\frac{\partial^2 T_{\mathrm{s}}}{\partial z^2} - hS(T_{\mathrm{s}}-T_{\mathrm{g}}) + \sum_{j=1}^{n\mathrm{Rct}} a_j(z)(-\Delta H)_j R_j(x_{\mathrm{g,in}}, T_{\mathrm{s}}). \tag{13}$$

Let us define the heat generation term in the above equation in a compact form as

$$F(T_{\mathrm{s}}) \equiv \sum_{j=1}^{n\mathrm{Rct}} a_j(z)(-\Delta H)_j R_j(x_{\mathrm{g,in}}, T_{\mathrm{s}}) \tag{14}$$

and cast Eq. 13 into a nondimensional form by defining the following dimensionless variables

$$\bar{T}_{\mathrm{s}} = \frac{(T_{\mathrm{s}}-T_0)}{\Delta T_{\mathrm{ref}}}, \quad \bar{z} = \frac{(z-z_0)}{\Delta z_{\mathrm{ref}}} \tag{15}$$

where in the interests of isolating the region in the vicinity of the light-off location, it is clear that $z_0 = z_{\mathrm{lo}}$ and $\Delta z_{\mathrm{ref}} = L$, whereas T_0 and ΔT_{ref} represent as yet undefined reference temperature scaling quantities that will be defined shortly in the analysis that follows. Combining the above scaled variables and the gas phase energy balance in Eq. 8 with Eq. 13 gives us

$$\varepsilon\frac{\partial^2 \bar{T}_{\mathrm{s}}}{\partial \bar{z}^2} - (1-\bar{F}')\frac{\partial \bar{T}_{\mathrm{s}}}{\partial \bar{z}} + B\bar{F} = 0 \tag{16}$$

where the dimensionless functional forms are

$$\bar{F}(\bar{T}_{\mathrm{s}}) = \frac{F(T_{\mathrm{s}})}{hS\Delta T_{\mathrm{ref}}}, \quad \bar{F}'(\bar{T}_{\mathrm{s}}) \equiv \frac{d\bar{F}}{d\bar{T}_{\mathrm{s}}} = \frac{dF/dT_{\mathrm{s}}}{hS}$$

and the dimensionless parameters of the problem that emerge are

$$\varepsilon = \frac{f_{\mathrm{sb}}\lambda_{\mathrm{sb}}/L}{wC_{\mathrm{p,g}}/A}, \quad \text{and} \quad B = \frac{hSL}{wC_{\mathrm{p,g}}/A}$$

The parameter ε is a measure of axial heat conduction in the substrate wall, while B a measure of heat convection at the wall-gas interface, both relative to the enthalpy flux of the flow. These parameters can be expressed in terms of their more commonly encountered channel flow counterparts as

$$\varepsilon = \frac{\lambda' D_{\mathrm{h}}/L}{Pe_{D_{\mathrm{h}}}} \quad \text{where} \quad \lambda' = \frac{f_{\mathrm{sb}}\lambda_{\mathrm{sb}}}{\lambda_{\mathrm{g}}} \quad \text{and} \quad Pe_{D_{\mathrm{h}}} = \frac{wC_{\mathrm{p,g}}/A}{\lambda_{\mathrm{g}}/D_{\mathrm{h}}}$$

$$B = St\,SL \quad \text{where} \quad St \equiv \frac{Nu_{D_{\mathrm{h}}}}{Pe_{D_{\mathrm{h}}}} \quad \text{and} \quad Nu_{D_{\mathrm{h}}} = \frac{hD_{\mathrm{h}}}{\lambda_{\mathrm{g}}}$$

where the standard channel flow definitions of the Nusselt ($Nu_{D_{\mathrm{h}}}$), Peclet ($Pe_{D_{\mathrm{h}}}$), and Stanton (St) numbers in terms of the hydraulic diameter have been invoked.

The parameter B is typically an $O(1)$ quantity in a converter, whereas by nature of its definition, the parameter ε is a small perturbation quantity ($\varepsilon \ll 1$). In the limit of $\varepsilon \to 0$ in Eq. 16 we lose the heat diffusion term and recover the nondimensional equivalent of Eq. 7 which can be solved to determine z_{lo} as a function of the parameter B as was done earlier to arrive at the result in Eq. 11.

However, to capture the role of axial conduction effects on the light-off zone, it is important to retain the diffusion term in Eq. 16 in our analysis. By virtue of the small parameter ε multiplying the second-order derivative heat diffusive term in Eq. 16, the solution for $\bar{T}_{\mathrm{s}}$ can be expected to exhibit classic "boundary layer" behavior. To analyze this behavior it is beneficial to employ the matched asymptotic technique using strained coordinates to magnify the region in the vicinity of $z = z_{\mathrm{lo}}$. To do so we define a local strained coordinate

$$\xi = \frac{\bar{z}}{g(\varepsilon)} = \frac{(z-z_{\mathrm{lo}})/L}{g(\varepsilon)}$$

and substitute it in Eq. 16 to determine that the magnifying scale above should be $g(\varepsilon) = \varepsilon$ to ensure a proper physical balance in Eq. 16 which becomes

$$\frac{\partial^2 \bar{T}_{\mathrm{s}}}{\partial \xi^2} - (1-\bar{F}')\frac{\partial \bar{T}_{\mathrm{s}}}{\partial \xi} + \varepsilon B\bar{F} = 0. \tag{17}$$

The solution of the above equation can be sought in the form of a perturbation series as

$$\bar{T}_{\mathrm{s}} = \bar{T}_{\mathrm{s}0} + \varepsilon\bar{T}_{\mathrm{s}1} + \varepsilon^2\bar{T}_{\mathrm{s}2} + \cdots$$

in which the leading order term $\bar{T}_{\mathrm{s}0}$ (in the limit of $\varepsilon \to 0$) is governed by

$$\frac{\partial^2 \bar{T}_{\mathrm{s}0}}{\partial \xi^2} - (1-\bar{F}'_0)\frac{\partial \bar{T}_{\mathrm{s}0}}{\partial \xi} = \mathcal{O}(\varepsilon) \tag{18}$$

and correctly provides a dominant balance between the diffusive and convective terms of the process in the local stretched coordinate frame of reference of $\xi \leq 0$. The leading order solution $\bar{T}_{\mathrm{s}0}$ of Eq. 18 can be determined subject to suitable boundary conditions which can be specified only

Table 1. Standard Physical Parameters and Operating Conditions

Property	Symbol	Units	Value
Monolith length	L	m	5.08×10^{-2}
Monolith frontal area	A	m^2	110.1×10^{-4}
Cell density	C_d	cpsi (cells per square inch)	600
Substrate thickness	w_{sb}	mils (milli inch)	3.5
Washcoat thickness	w_{wc}	μm (microns)	30
Specific heat capacity of the gas	$c_{p,g}$	J/mol/K	30
Substrate thermal conductivity	λ_{sb}	W/m/K	1.5
Nusselt/Sherwood number	*Nu, Sh*	–	2.97
Catalyst surface area	a_j	m^2/L	7.4
Inlet mass flow rate	–	g/s	15
Inlet gas temperature	$T_{g,in}$	K	600
Inlet mole fraction of CO	$x_{g,in,\ CO}$	–	2%
Inlet mole fraction of C_3H_6	$x_{g,in,\ C_3H_6}$	–	450 ppm
Inlet mole fraction of C_3H_8	$x_{g,in,\ C_3H_8}$	–	50 ppm
Inlet mole fraction of H_2	$x_{g,in,\ H_2}$	–	0.667%
Inlet mole fraction of O_2	$x_{g,in,\ O_2}$	–	1.8%
Inlet mole fraction of NO	$x_{g,in,\ NO}$	–	1,000 ppm

after the proper temperature scaling in Eq. 15 is first established. Because of the nature of the diffusive effects we are trying to capture in the region $z < z_{lo}$, i.e. $\xi < 0$, and extending up to $\xi \to 0$, the appropriate temperature reference quantities in Eq. 15 should be $T_0 = T_{s,in}$ and $\Delta T_{ref} = (T_{s,lo} - T_{s,in})$ so that the corresponding boundary conditions for $\bar{T}_s$ in Eq. 17 in terms of the stretched coordinate ξ become suitably normalized to

$$\bar{T}_s = 0 \quad \text{as} \quad \xi \to -\infty, \quad \text{and} \quad \bar{T}_s = 1 \quad \text{as} \quad \xi \to 0. \quad (19)$$

Since by definition $\bar{F}$ is a function of $\bar{T}_s$, Eq. 17 is a fully nonlinear equation in $\bar{T}_s$ and does not permit a simple closed form analytical solution for $\bar{T}_s(\xi)$. However for the leading order solution $\bar{T}_{s0}(\xi)$ governed by Eq. 18, neglecting the $\bar{F}'$ term as a first approximation and doing a quick analysis subject to Eq. 19 yields a leading order solution behavior nominally of the type $\bar{T}_{s0} \approx e^{\xi}$ which suggests a front thickness that is diffused over a length scale of $\mathcal{O}(\varepsilon L)$. The parameter ε defined by $\frac{f_{sb}\lambda_{sb}/L}{wC_{p,g}/A}$ is representative of the relative magnitude of the axial heat conduction flux in the solid substrate to the enthalpy flux in the flow and is hence a measure of the localization of the light-off region. A more complete solution and discussion (of the nature of $\bar{T}_s(\xi)$) based on a detailed numerical analysis of the light-off zone will be presented in the following section for a specific representative case of a TWC converter for which a simplified set of reactions and kinetics available in the literature have been used.

Results and Analysis

In this section, the effects of important operating and design variables on the light-off behavior (both the light-off location and the spread of the light-off front for finite solid conduction) are analyzed for the case of a representative set of oxidation reactions in a TWC. For purposes of simplicity and clarity, a representative set of reactions and kinetics (available in the literature) have been chosen primarily to illustrate the range of competing factors in a multireaction system and demonstrate the applicability of the analysis developed in this study. Note that the entire complex set of reactions of a modern TWC has not been considered here and hence the results are not a completely quantitatively accurate reflection of a modern TWC.

The main representative reactions and their kinetics considered here have been taken from the literature[26] and are listed below:

$$CO + 0.5O_2 \rightarrow CO_2$$
$$C_3H_6 + 4.5O_2 \rightarrow 3CO_2 + 3H_2O$$
$$C_3H_8 + 5O_2 \rightarrow 3CO_2 + 3H_2O$$
$$H_2 + 0.5O_2 \rightarrow H_2O.$$

The only other nonreacting species in the reactor in this example is NO. Though NO reduction reactions (with carbon monoxide, hydrocarbons, hydrogen) are important, for the purpose of simplicity we do not consider these reactions in this work. Unless mentioned otherwise, we use the standard set of parameters listed in Table 1 for the numerical analysis from which the baseline value for the catalyst active surface area loading parameter a_j can be calculated to be 7.4 m^2/L of converter volume. The formulas used to calculate D_h, f_{sb} are listed in Table 2. It may be noted that not all of the values in Table 1 are in SI units since units used in common practice have also been used.

Figure 2 shows the influence of the inlet gas temperature on light-off location for a representative case as indicated in the caption. It can be observed that as the inlet gas temperature increases, the light-off location moves upstream toward the inlet. When the inlet gas temperature has a value of 815 K, light-off occurs at a $z_{lo} = 10^{-3}$ m which can be taken to be essentially at the inlet. It can be verified that this means that the condition in Eq. 12 noted earlier is satisfied. Also, if the monolith reactor is, say 0.1-m long (represented by the horizontal dotted line in Figure 2), then for any inlet gas tempera-

Table 2. Formulas Used to Calculate Other Parameters

Parameter	Units	Formula
D_h	m	$1/\sqrt{C_d} - 2w_{wc} - w_{sb}$
S	m^2/m^3	$4C_dD_h$
f_{sb}	–	$w_{sb}\sqrt{C_d}(2 - w_{sb}\sqrt{C_d})$

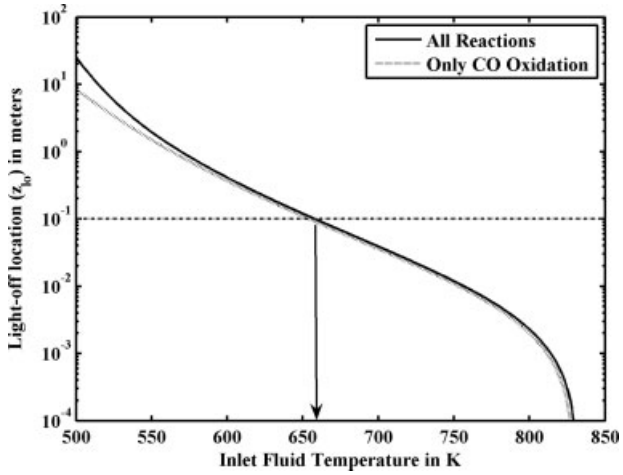

Figure 2. Influence of inlet gas temperature on the light-off location for the standard set of parameter values listed in Table 1.

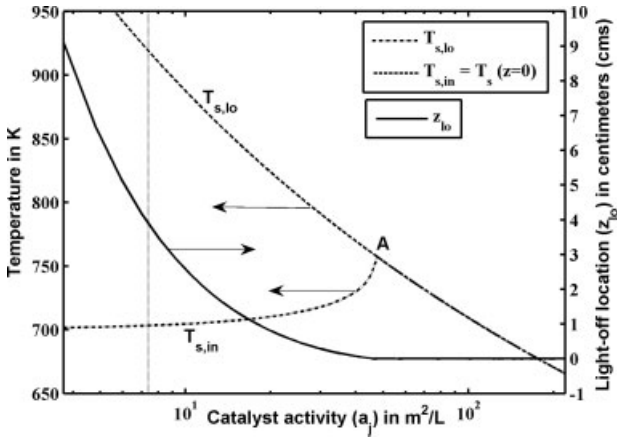

Figure 3. Variation of the inlet solid temperature, the light-off temperature and the location of light-off as a function of catalyst activity (for $T_{g,in}$ = 700 K).

ture less than 657 K (this threshold value would be 628 and 612 K for a 0.2- and 0.3-m long reactor, respectively), there is no light-off within the reactor. In other words the minimum inlet gas temperature required for light-off in a 0.1-m long reactor is 657 K. So as we increase the inlet gas temperature from its minimum value, the light-off behavior changes from a no light-off condition, to a near-exit light-off condition, to eventually a near-inlet light-off condition at a high enough inlet gas temperature as the light-off location moves upstream. Figure 2 also shows the influence of the hydrocarbon and hydrogen oxidation reactions on the light-off behavior. When the hydrocarbons and hydrogen are removed from the feed (inlet gas stream), there is no significant change in the light-off behavior, indicating the dominant role of the CO oxidation reaction. It should be noted that this observation (that hydrogen and hydrocarbons in the feed have little impact on the light-off behavior) is very specific to the example considered here and cannot be generalized. However, a similar type of analysis can be performed for any other system to arrive at similar conclusions by using a suitable model to predict light-off such as in Eq. 11 developed in this work.

Figure 3 illustrates the variation of the inlet solid temperature, the light-off temperature, and the light-off location as we change the catalyst active surface area (a_j) for the standard set of parameters in Table 1 and a representative inlet gas temperature ($T_{g,in}$) of 700 K. The dotted vertical line shows the default baseline value of a_j that is being used. At lower values of a_j, the inlet solid temperature is low, the light-off temperature is high, and the light-off location is far downstream of the inlet. As we increase the catalyst activity, the inlet solid temperature increases, the light-off temperature decreases, and the light-off location moves upstream toward the inlet. At a certain large enough value of a_j, the inlet solid temperature becomes equal to the light-off temperature and the light-off occurs at the inlet. This point is denoted by A in Figure 3. For values of a_j greater than this value, the inlet solid temperature and the light-off temperature continue to remain equal but decrease in magnitude, whereas the light-off location remains at zero.

Figure 4 shows the inlet gas temperature required for near-inlet light-off as a function of the catalyst activity with all other parameters fixed at the standard values listed in Table 1. In this figure, the inlet gas temperature for near-inlet light-off is calculated using two approaches. The first approach is to solve for $T_{g,in}$ using the equality condition in Eq. 12 (which implies $z_{lo} = 0$) and the second approach is to solve for $T_{g,in}$ using Eq. 11 with $z_{lo} = 10^{-3}$ m chosen (somewhat arbitrarily) as a realistic near-inlet value. As shown in the figure, there is a difference between the required inlet gas temperatures of about 10–20 K for these two cases depending on the catalyst activity. Also shown in the figure for ease of understanding is the variation of the corresponding solid light-off temperature, which under these conditions of near-inlet light off is essentially equal to the solid inlet temperature.

Figure 5 shows the variation of the light-off location with catalyst activity and shows that it moves upstream with increasing catalyst loading for a given inlet gas temperature.

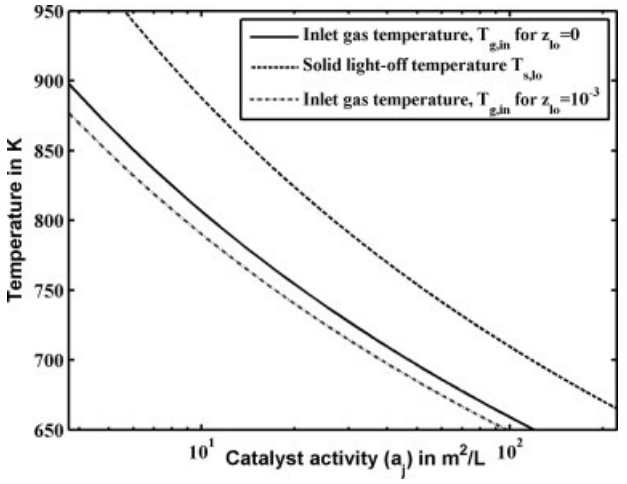

Figure 4. Inlet gas temperature required for near-inlet light-off as a function of the catalyst activity.

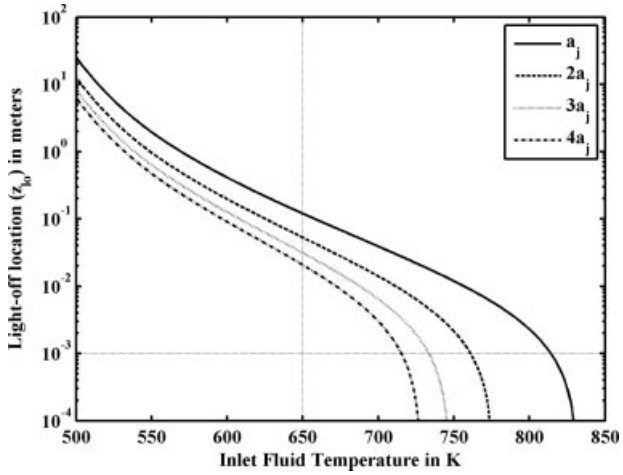

Figure 5. Influence of catalyst activity on the variation of the light-off location as a function of the inlet gas temperature.

The vertical line at 650 K (for example) shows how much closer to the inlet the light-off occurs as we double, triple, and quadruple the catalyst activity relative to its baseline value in Table 1. The figure also shows the minimum inlet gas temperature required for near-inlet light-off defined as $z_{lo} = 10^{-3}$ m (indicated by the horizontal line in the figure). For instance, doubling the catalyst activity decreases the minimum inlet gas temperature required for near-inlet light-off by about 45 K and tripling the catalyst activity reduces it by 80 K relative to the baseline value for the model problem considered in this study.

Figure 6 shows the inhibition effect of NO on light-off behavior. As mentioned earlier in this section, the NO inhibition of the oxidation reactions appears through the reaction rate expressions[26] even though NO is a nonreacting species. As can be seen from the figure, there is a significant impact on the light-off temperature and location due to the presence of NO in the feed. With 1000 ppm of NO, the inlet temperature required for near-inlet light-off (defined earlier as $z_{lo} = 10^{-3}$ m) is about 815 K, but when we reduce the NO concentration by half, the temperature required for near-inlet light-off reduces by 40 K. The significant effect of the influence of the NO concentration is seen in the 0–100 ppm range where the inlet temperature required for near-inlet light-off decreases by more than 70 K indicating a logarithmic type dependence of the inhibition effect on the NO concentration.

The results in Figures 1–6 can be captured in the trends shown in Scheme 1. For example, for a given monolith and flow conditions, at a certain inlet gas temperature $T_{g,in}^{(1)}$, light-off occurs at the location $z_{lo}^{(A)}$ for a certain catalyst loading condition of $a_j^{(A)}$. At this location, the solid temperature (which remains almost constant at its inlet value up to this point), jumps to the light-off value as indicated by the bold arrows in the schematic. Increasing the catalyst loading to $a_j^{(B)}$ or to $a_j^{(C)}$ moves the z_{lo} location further upstream and changes the solid temperature variation and reduces the jump as shown (corresponding to the locations $z_{lo}^{(B)}$ and $z_{lo}^{(C)}$), until a loading condition ($a_j^{(max)}$) is reached at which light-off occurs at the inlet ($z_{lo} = 0$) and the corresponding temperature jump is zero. For a different inlet gas temperature $T_{g,in}^{(2)} > T_{g,in}^{(1)}$ the resulting trends are shifted as shown in the schematic, although the corresponding values of a_j required to achieve this condition at each of the z_{lo} locations shown in the schematic are lower for the higher inlet gas temperature.

Figures 7 and 8 deal with the spread of temperature in the light-off zone due to heat diffusion in the substrate for which the governing equations were developed at the end of the previous section. Here we look at the complete numerical solution of the temperature distribution $\bar{T}_s(\xi)$ governed by Eq. 17 to understand the nature and extent of the diffusion of the front for some representative cases corresponding to the results shown in Figures 1–6. We continue to use the standard reference set of parameters from Table 1.

Figure 7 shows the nature of the temperature spread in the light-off front as a function of different catalyst loading values for a standard case of a monolith with a cell density of 600 cpsi and substrate thickness of 3.5 mils (0.0889 mm) indicated in Table 1. The dotted line is the simple e^{ξ} approximate solution to Eq. 17 (suggested at the end of the previous section) while the solid curves are the full numerical solution for different loading values indicated on the figure. It is clear that the reaction front thickens significantly with increasing loading as the light-off location moves upstream to a near-inlet condition.

Figure 8 shows the nature of the temperature spread in the light-off front as a function of monolith cell density C_d and substrate thickness w_{sb} for a reference case of a uniform catalyst loading value of $20a_j$. The dotted line is the simple e^{ξ} approximate solution to Eq. 17 while the solid curves are the full numerical solution for different typical cell density values used in practice as indicated on the figure. It is again clear that the reaction front thickens with decreasing C_d (since the role of w_{sb} is absorbed into ε as discussed in the following paragraph) as the light-off location moves upstream to a near-inlet condition.

The trends shown in Figures 7 and 8 can be explained by first noting that the dominant contribution to the temperature solution in the vicinity of the light-off location ($\xi = 0$)

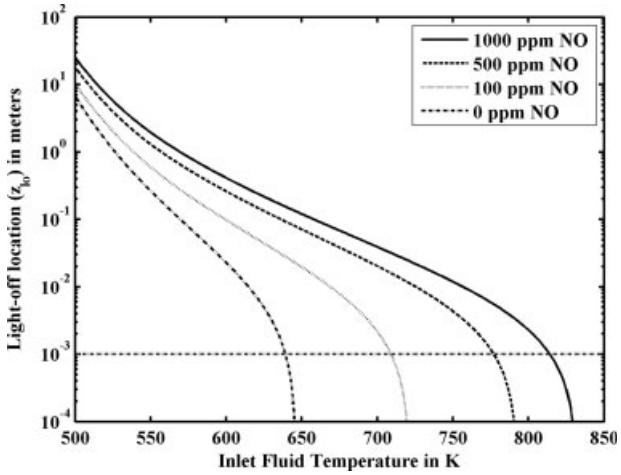

Figure 6. Influence of NO concentration on the variation of the light-off location as a function of the inlet gas temperature.

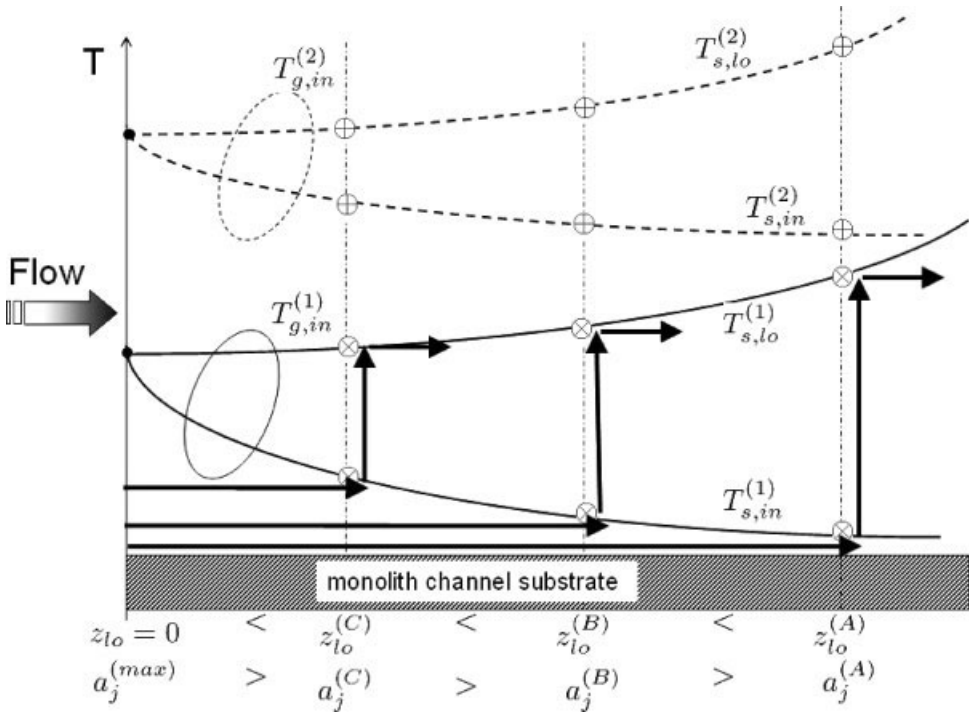

Scheme 1. Trends in the variation of the solid inlet temperature ($T_{s,in}$) and the light-off temperature ($T_{s,lo}$) at the light-off location (z_{lo}), as a function of catalyst loading (a_j), for two different inlet gas temperatures ($T_{g,in}^{(1)} < T_{g,in}^{(2)}$).

comes from the leading order term $\bar{T}_{s0}$ which is governed by Eq. 18. The behavior of this leading order term is determined by the nature of $\bar{F}'$ present in Eq. 18 which has a functional dependence given by $\bar{F}' \sim a_j/hS$. By definition, $hS = 4Nu_{D_h}\lambda_g C_d$ (in which Nu_{Dh} and λ_g are assumed constant) thereby indicating a variation in these curves that simply scales through the ratio a_j/C_d, i.e. for increasing values of this ratio the zone front thickens as the light-off location moves upstream to a near-inlet condition (and vice versa). It is important to note that the effect of the kinetics and activation energies of the chosen reaction set are captured in the $\bar{F}'$ term present in Eq. 18 and are critical in determining the profiles in Figures 7 and 8. As for some of the other variables in the problem such as flow rate, w, monolith frontal area, A, substrate thickness, w_{sb}, (which determines f_{sb}) or substrate thermal conductivity, λ_{sb}, the effects of these variables

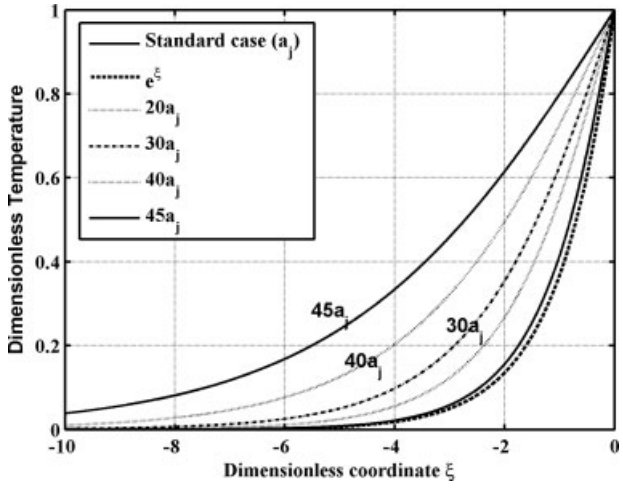

Figure 7. Variation of the dimensionless temperature ($\bar{T}_s$) and spread of the reaction front as a function of catalyst loading (a_j).

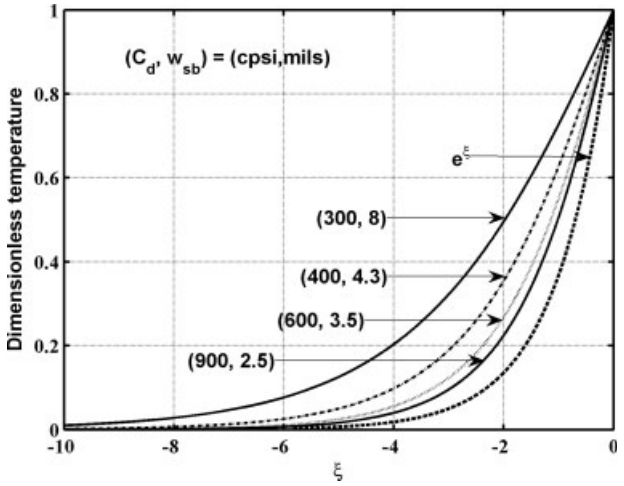

Figure 8. Variation of the dimensionless temperature ($\bar{T}_s$) and spread of the reaction front as a function of monolith cell density (C_d) and substrate thickness (w_{sb}) for a catalyst loading of $20a_j$.

are essentially factored into the parameter ε which is absorbed in the problem scaling leading to Eq. 17.

The curves in Figures 7 and 8 can also be used to estimate the actual dimensional front thickness and study its dependence on the different parameters in the problem. Let us first define the front thickness based on a consistent (although somewhat arbitrary but commonly used) criterion as the location corresponding to a 99% decay in a given temperature curve, i.e. as the ξ–location at which $\bar{T}_s = 0.01$. It is clear then from these curves that the front thickness is of the $\mathcal{O}(5-10)$ in units of ξ depending on the value of a_j or C_d. By definition of ξ this corresponds to a dimensional thickness of $\mathcal{O}([5-10]\varepsilon L)$ where the definition

$$\varepsilon L = \frac{f_{sb}\lambda_{sb}}{wC_{p,g}/A}$$

indicates the presence of a front thickness length scale which is a function of only the substrate and flow properties in the problem. For the curves in Figures 7 and 8 the front thickness can be calculated and shown to be in the range of about 1–3 mm (depending on the value of a_j or C_d) which is representative of the spread of the temperature profile in the light-off front. The significance of this result will be discussed further in the following section.

Discussion

Many chemical reacting systems exhibit light-off behavior, or "thermal run-away" as it is sometimes called. In certain systems such a behavior is preferred (say, where maximum conversion is desired) and in some systems it is not (say, to avoid high temperatures, etc). In this work, we examine light-off behavior (characterized by the light-off location and thickening of the light-off front) in a catalytic monolith reactor for the general case of multiple reactions and generalized kinetics. A one-dimensional two-phase model has been developed for a monolith reactor and techniques from nonlinear analysis are applied to this model to arrive at an analytical expression in Eq. 11 to determine the light-off location. This analytical expression contains all the important operating and design variables of the monolith reactor and also the reaction specific variables such as the kinetic parameters and the heats of reaction. We first obtain the light-off location analytically assuming negligible solid conduction, and then extend the applicability to estimate the spread of the light-off front by including finite conduction in the solid substrate. This study can be used to model and quantitatively study light-off behavior accurately without having to numerically solve the entire set of governing partial differential equations.

The TWC example

A specific representative case of a TWC converter for which a simplified set of reactions and kinetics are available in the literature[26] is used to illustrate the application of this work. Detailed analyses are performed to study the light-off behavior and to quantify the influence of the various design and operating variables. Some of the important observations are that (a) as we increase the inlet gas temperature, the light-off behavior changes from no light-off in a given reactor to near-exit light-off to near-inlet light off, (b) for a typical case doubling or tripling the catalyst activity decreases the minimum inlet gas temperature required for near-inlet light-off significantly, (c) the NO inhibition effect is important and especially so for lower NO concentrations, (d) the spread of the light-off front is of the order $\mathcal{O}([5-10]\varepsilon L)$ where

$$\varepsilon L = \frac{f_{sb}\lambda_{sb}}{wC_{p,g}/A}$$

and for typical values of the operating conditions this front thickness is around 1–3 mm. While some of these results are very specific to this system (and/or parameters chosen), these results provide insight into how the analysis presented in this work could be used to study light-off behavior in a general chemically reacting system. Rather than dwell on the case-specific numerical results considered here, we would like to focus on how such an approach can be generalized to arrive at some useful design guidelines that can be implemented to improve the performance of catalytic monolith reactors.

Transient analysis for a more general case

In most automobile exhaust gas aftertreatment systems (used in the control of emissions) such as TWC, DOC, LNT, SCR, etc., we would like to achieve early light-off and high conversion efficiencies for better emissions performance. Though the analysis presented in this work was for steady state conditions, we can extend some of these results to transient behavior as well. As noted in the section on light-off, its location (z_{lo}) obtained using Eq. 11 can also be viewed as the location in the reactor that would light-off first (in time). In a transient situation, the solid has to be heated to the light-off temperature by the flowing gas with the help of the heat of reactions. For the case of negligible solid conduction in the monolith, the little heat generated by the reaction in the early stages before light-off does not spread in the solid and is localized, though it can be transferred to the gas by convection at a particular location. This helps the localized solid catalyst to reach the light-off temperature early as only the localized region needs to be heated to the required extent. But when there is finite solid conduction, the heat generated before light-off starts to diffuse in the solid (in addition to being transferred to the gas) and hence more heat (and hence more time) is needed for the solid catalyst to reach the light-off temperature. So with finite solid conduction, we need to heat a sufficient mass of the solid substrate/catalyst before it can reach the light-off temperature/condition. This mass can be estimated from the thickness of the light-off front which was found earlier to be typically $\mathcal{O}([5-10]\varepsilon L)$ and shows that as conduction in the solid increases, the spread of the light-off front also increases and the localized feature of the light-off zone is diminished. More significantly, this in turn increases the time required for light-off as more heat is needed (because of the increased thermal mass due to increased temperature spread) for the solid to reach the light-off temperature. So for metallic substrates that typically have conductivity values 10–15 times that of ceramic substrates, the thickness of the light-off zone, which scales directly with the substrate thermal conductivity, will also be 10–15 times as much, thereby increasing the thermal mass that needs to

be heated before the solid reaches the light-off temperature. For typical parameter values, the resulting thickness of the light-off front could be as much as 10–30 mm for metallic substrates. However if the enthalpy flux of the flow is sufficiently high (due to large flow rate and/or small monolith frontal area) such that we maintain a small ε parameter value, we could still have a small light-off front thickness even with metallic substrates. From the above discussion, it is clear that it is always desirable to be in the regime of small ε so as to have localized as well as early light-off behavior. As mentioned earlier, we discuss the limiting case of infinite solid conductivity in the substrate walls and its effect on the light-off behavior in an Appendix.

Although typical engine exhaust aftertreatment devices (such as a TWC or DOC) do not have constant inlet conditions as has been assumed in this work, the analysis shown here could nonetheless be applied to such cases. When the inlet conditions change with time, one of the approaches could be to get an average value of the inlet concentrations and use this to calculate an "effective inlet gas temperature" required for near-inlet light-off. In a typical automotive engine drive cycle where the inlet gas temperature keeps increasing with time, we could find the time at which the "effective inlet gas temperature" reaches a prescribed value required for near-inlet light-off. This time can then be minimized by changing various design parameters to arrive at an optimum set of parameters that would favor near-inlet light-off at lower inlet gas temperatures (which means less time). The parameters that could be changed to have a near-inlet light-off at a given inlet gas temperature were discussed earlier with reference to Eq. 12.

Light-off location and the role of catalyst loading

From a transient as well as a steady state point of view, there are clear advantages to having the light-off close to the inlet as compared to a light-off further downstream in the reactor. This has been discussed in detail.[32] As mentioned earlier, the conversion in the reactor is determined by the lit-off region of the monolith ($L - z_{lo}$) (which is in the high temperature branch) and hence having a smaller z_{lo} is desirable for higher conversions. From a transient behavior point of view, when the light-off occurs close to the inlet, the time taken for the rest of the reactor to light-off is considerably smaller because the heat generated after light-off can be transported downstream both by convection in the gas and conduction in the solid walls. On the other hand if the light-off occurs at any location (z_{lo}) downstream of the inlet, the primary mode of heat transfer upstream of that location is only heat conduction in the monolith. Since heat conduction time scales are typically larger compared to the convection time scales in the gas, it takes significantly more time for the region upstream of z_{lo} to also achieve the light-off condition. Hence the overall conversion efficiency of the monolith which is essentially due to the lit-off region would not be as high (as compared to the case where there is light-off near the inlet and the entire monolith is therefore in a lit-off state).

Note that to favor a near-inlet light-off we need a high enough catalyst loading only close to the inlet, while in the remainder of the reactor it can be held at a suitable minimum value so that the reactor is maintained in the mass transfer-controlled regime. However in practical applications there is considerable deactivation of the catalyst primarily near the inlet (thus lowering the effective value of a_j near the inlet) and the developing thermal entrance region of the flow results in a higher Nusselt number (and hence higher h). Both these factors act as deterrents for near-inlet light-off as evident from the criterion in Eq. 12. Hence, it may be advisable to have the light-off location downstream of the developing entry region or sufficiently downstream of the inlet to compensate for the above effects.

Effect of external heat loss

In many applications, the monolith reactor is not adiabatic and there is significant external heat transfer between the converter canister and its surroundings. A simple but approximate way to model this phenomenon using a one-dimensional model is to relax the adiabatic assumption and add an external heat loss in the solid energy balance. As a result the solid phase energy balance for the channel walls in Eq. 1 is modified to

$$\left(f_{sb}\rho_{sb}C_{p,sb} + f_{wc}\rho_{wc}C_{p,wc}\right)\frac{\partial T_s}{\partial t} = f_{sb}\lambda_{sb}\frac{\partial^2 T_s}{\partial z^2} + hS(T_g - T_s) - \sum_{j=1}^{nRct} a_j(z)(\Delta H)_j R_j - h_L S_L(T_s - T_a) \quad (20)$$

where h_L is the external heat transfer coefficient, T_a is the ambient temperature, and S_L is the external surface area of the reactor per unit reactor volume available for external heat transfer with the ambient. Although the above equation cannot capture the exact quantitative heat-loss behavior in a catalytic monolith it captures the qualitative behavior through this additional heat loss term. Since the above equation along with Eqs. 2 and 3 are an exact representation of the science at the single channel level, it may be noted that the entire analysis in this work is fully applicable to tubular reactors with wall reactions on an exact basis at the single channel level, in addition to being valid for complete catalytic reactors on an approximate basis at the complete monolith level. It should be mentioned that the significance of the heat loss from a monolith reactor is very application specific[46] and depends on the monolith properties, the reaction system, and the test procedure and/or conditions.

The analysis presented earlier can be extended to this case and the light-off location (given earlier by Eq. 11) can be obtained as

$$z_{lo} = \frac{wC_{p,g}}{hSA}\ln\left(\frac{\sum_{j=1}^{nRct} a_j(\Delta H)_j R_j(x_{g,in}, T_{s,in}) + h_L S_L(T_{s,in} - T_a)}{\sum_{j=1}^{nRct} a_j(\Delta H)_j R_j(x_{g,in}, T_{s,lo}) + h_L S_L(T_{s,lo} - T_a)}\right) + \frac{wC_{p,g}}{A}\int_{T_{s,in}}^{T_{s,lo}} \frac{dT_s}{\sum_{j=1}^{nRct} a_j(-\Delta H)_j R_j(x_{g,in}, T_s) + h_L S_L(T_s - T_a)} \quad (21)$$

where $T_{s,in}$ is obtained by solving

$$hS(T_{g,in} - T_{s,in}) - h_L S_L(T_{s,in} - T_a) - \sum_{j=1}^{nRct} a_j(\Delta H)_j R_j(x_{g,in}, T_{s,in}) = 0$$

and $T_{s,lo}$ is obtained by solving

$$- hS - h_L S_L - \sum_{j=1}^{nRct} a_j (\Delta H)_j \frac{d}{dT_s} \left(R_j(x_{g,in}, T_s) \right) = 0.$$

Here again, it is assumed that even with heat-loss from the reactor, there still exists an ignition or light-off point in the feasible region as defined earlier in the context of this study. (Note: It is possible for the light-off point to disappear with heat losses in the system although we do not consider such cases in this study as noted earlier). As can be expected, the additional heat loss to the surroundings makes it more difficult to achieve light-off because it results in the need for an increased light-off temperature. This is because the heat of reaction generated before light-off is now being lost by an additional heat transport mechanism and has to be compensated. So for a given set of parameters, the light-off location will move further downstream for a case with external heat loss compared to an adiabatic case. Along similar lines, the criterion for near-inlet light-off (earlier given by Eq. 12) can be modified to

$$\frac{\sum_{j=1}^{nRct} a_j (-\Delta H)_j R_j(x_{g,in}, T_{s,lo})}{hS(T_{s,lo} - T_{g,in}) + h_L S_L (T_{s,lo} - T_a)} \geq 1$$

and reconfirms the fact that external heat loss hampers light-off and we need higher inlet gas temperatures and/or higher catalyst loading for near-inlet light-off compared to the adiabatic case. Interestingly enough, the additional external heat loss term does not have a significant effect on the thickness of the light-off front and the spread is still characterized by the parameter ε. This is because the external heat loss term represents heat transport in the transverse direction between the surface and the ambient, while heat diffusion effects in the solid wall are mainly in the streamwise (or flow) direction. The analysis performed earlier on the spread holds for this case as well with a small modification in the definition of F (earlier given by Eq. 14) as follows

$$F(T_s) \equiv \sum_{j=1}^{nRct} a_j(z) \, (-\Delta H)_j \, R_j(x_{g,in}, T_s) - h_L S_L (T_s - T_a).$$

So while the light-off is delayed with external heat loss, the spread of the light-off front remains essentially unchanged. A more detailed analysis can be performed using the above equations to fully quantify the effect of external heat loss although we do not attempt to do so in this work.

Closing comments

The above discussion provides various pointers for better design of catalytic monoliths that favor (early) light-off. To avoid early light-off in a reactor system application, many of the above conclusions could be reversed using the formulas and analysis in the sections on light-off and spread. The generalized approach to studying light-off behavior used in this work also helps in analyzing how the reaction kinetics and/or species concentrations affect the light-off behavior in addition to studying the influence of the various design and operating parameters. In general, the results and inferences from this work could be used to determine optimal operating, design, and reaction conditions for improved performance of monolith reactors. This work could also be extended for application to regeneration in diesel particulate filters (DPFs) to determine the minimum inlet gas temperature (which is effectively the amount of heat/fuel that has to be added upstream of the DPF) that is required to achieve a desired degree of soot oxidation. Though the results obtained in this work can be qualitatively applied to transient cases as discussed earlier, a more comprehensive analysis would be required to extend the applicability completely to a wider range of operating conditions to capture the full transient behavior of reactor systems.

Acknowledgments

The authors thank K. Raghunathan of the India Science Lab, GM Research and Development center for the helpful discussions, suggestions and comments on this work. The authors also thank Edward J. Bissett and Se H. Oh of the Chemical and Environmental Sciences lab, GM Research and Development center for providing valuable comments and feedback on the section on light-off location of this work. Feedback from the reviewers helped clarify certain points and is appreciated.

Notation

a_j = catalyst surface area per unit volume of the monolith (m^2/m^3)
A = monolith frontal area (m^2)
c = total molar concentration (mol/m^3)
$C_{p,g}$ = specific heat capacity of gas (J/mol/K)
$C_{p,sb}$ = specific heat capacity of the substrate (J/kg/K)
$C_{p,wc}$ = specific heat capacity of the washcoat (J/kg/K)
C_d = cell density ($cells/m^2$)
D_h = hydraulic diameter (m)
$D_{i,m}$ = mass diffusivity of the i^{th} species (m^2/s)
f_{sb} = volume fraction of the substrate in the monolith
f_{wc} = volume fraction of the washcoat in the monolith
h = heat transfer coefficient between solid and gas ($J/m^2/s/K$)
h_L = external heat transfer coefficient between solid and ambient ($J/m^2/s/K$)
$k_{m,i}$ = mass transfer coefficient between solid and gas for ith species ($mol/m^2/s$)
L = length of the monolith (m)
M_i = molecular weight of the ith species (g/mol)
Nu = Nusselt number
Pe_{D_h} = heat peclet number
R_g = universal gas constant (J/mol/K)
R_j = reaction rate for jth reaction ($mol/m^2/s$)
s_{ij} = stoichiometric coefficient of ith species in reaction j
S = surface area of solid substrate per monolith volume (m^2/m^3)
S_L = external radial surface area of reactor per monolith volume (m^2/m^3)
Sh = Sherwood number
St = Stanton number
t = time (s)
T = temperature (K)
$\bar{T}_s$ = dimensionless solid temperature
w = molar flow rate of inlet gas (mol/s)
w_{sb} = substrate thickness (m)
w_{wc} = washcoat thickness (m)
x = mole fraction of species
z = axial coordinate (m)
$\bar{z}$ = dimensionless axial coordinate
z_{lo} = light-off location (m)

Greek letters

$(\Delta H)_j$ = heat of reaction for reaction j (<0 for exothermic) (J/mol)
λ_g = thermal conductivity of the gas (W/m/K)

λ_{sb} = thermal conductivity of the substrate (W/m/K)
ξ = dimensionless axial coordinate
ρ_{sb} = subtrate density (kg/m^3)
ρ_{wc} = washcoat density (kg/m^3)

Subscripts and superscripts

a = ambient
g = gas phase
i = *i*th species
in = inlet
init = initial
j = *j*th reaction
lo = light-off
s = solid phase
sb = substrate

Literature Cited

1. Lox ESJ, Engler BH. Environmental catalysis. In: Ertl G, Weitkam J, Knozinger H, editors. *Handbook of Heterogeneous Catalysis, Vol. 4*. New York: Wiley,1997:1559–1633.
2. Cybulski A, Moulijn JA. Monoliths in heterogeneous catalysis. *Catal Rev Sci Eng*. 1994;36:179–270.
3. Groppi G, Tronconi E, Forzatti P. Mathematical models of catalytic combustors. *Catal Rev Sci Eng*. 1999;41:227–254.
4. Hayes RE, Kolaczkowski ST. *Introduction to Catalytic Combustion*. The Netherlands: Gordon and Breach Science Publishers, 1997.
5. Becker EG, Pereira CJ. *Computer Aided Design of Catalysts*. New York: Marcel Dekker, 1993.
6. Kašpar J, Fornasiero P, Hickey N. Automotive catalytic converters: current status and some perspectives. *Catal Today*. 2003;77:419–449.
7. Nijhuis TA, Beers AEW, Vergunst T, Hoek I, Kapteijn F, Moulijn JA. Preparation of monolithic catalysts. *Catal Rev Sci Eng*. 2001; 43:345–380.
8. Morgan CR, Carlson DW, Voltz SE. Thermal response and emission breakthrough of platinum monolithic catalytic converters. SAE Technical Paper Series. Paper No. 730569. 1973.
9. Young LC, Finlayson BA. Mathematical models of monolith catalytic converters. *AIChE J*. 1976;22:343–353.
10. Heck RH, Wei J, Katzer JR. Mathematical modeling of monolithic catalysts. *AIChE J*. 1976;22:477–484.
11. Boersma MAM, Tielen WHM, Baan HSVD. Experimental and theoretical study of simultaneous development of the velocity and concentration pro7les in the entrance region of a monolithic converter. *ACS Symp Ser*. 1978;65:72–82.
12. Chen DKS, Bissett EJ, Oh SH, Ostrom DLV. A three-dimensional model for the analysis of transient thermal and conversion characteristics of monolithic catalytic converters. SAE Techical Paper Series. Paper No. 880282. 1988.
13. Hayes RE, Kolaczkowski ST, Thomas WJ. Finite-element model for a catalytic monolith reactor. *Comput Chem Eng*. 1992;16:645–657.
14. Zygourakis, K. Design of monolithic catalysts for improved transient performance, In: Becker ER, Pereira CJ, editors. *Computer Aided Design of Catalysts*. New York: Marcel Dekker,1993:297–334.
15. Siemund S, Leclerc JP, Schweich D, Prigent M, Castagna F. Three-way monolithic converter: simulations versus experiments. *Chem Eng Sci*. 1996;51:3709–3720.
16. Koltsakis GC, Konstantinidis PA, Stamatelos AM. Development and application range of mathematical models for 3-way catalytic converters. *App Catal B: Environ*. 1997;12:161–191.
17. Jahn R, Snita D, Kubícek M, Marek M. 3-D modeling of monolith reactors. *Catal Today*. 1997;38:39–46.
18. Ohsawa K, Baba N, Kojima S. Numerical prediction of transient conversion characteristics in a three-way catalytic converter, SAE Technical Paper Series. Paper No. 982556. 1998.
19. Dubien C, Schweich D, Mabilon G, Martin B, Prigent M. Three-way catalytic converter modelling: fast- and slow-oxidizing hydrocarbons, inhibiting species, and steam-reforming reaction. *Chem Eng Sci*. 1998;53:471–481.
20. Jeong S-J, Kim W-S. A numerical approach to investigate transient thermal and conversion characteristics of automotive catalytic converter, SAE Technical Paper Series. Paper No. 980881. 1998.
21. Shamim T, Shen H, Sengupta S, Son S, Adamczyk AA. A comprehensive model to predict three-way catalytic converter performance. *J Eng Gas Turbines Power*. 2002;124:421–428.
22. Chakravarthy VK, Conklin JC, Daw CS, D'Azevedo EF. Multi-dimensional simulations of cold-start transients in a catalytic converter under steady inflow conditions. *Appl Catal A: General*. 2003; 241:289–306.
23. Koci P, Kubicek M, Marek M. Modeling of three-way-catalyst monolith converters with microkinetics and diffusion in the washcoat. *Ind Eng Chem Res*. 2004;43:4503–4510.
24. Depcik C, Assanis D. One-dimensional automotive catalyst modeling. *Prog Energy Combust Sci*. 2005;31:308–369.
25. Ahmadinejad M, Desai MR, Watling TC, York APE. Simulation of automotive emission control systems. *Adv Chem Eng*. 2008;33:47–101.
26. Oh SH, Cavendish JC. Transients of monolithic catalytic converters: responses to step changes in feed stream temperature as related to controlling automobile emissions. *Ind Eng Chem Prod Res Dev*. 1982;21:29–37.
27. Oh SH, Bissett EJ, Battiston PA. Mathematical modeling of electrically heated monolith converters: model formulation, numerical methods, and experimental verification. *Ind Eng Chem Res*. 1993;32:1560–1567.
28. Tronconi E, Forzatti P. Adequacy of lumped parameter models for SCR reactors with monolithic structures. *AIChE J*. 1992;38:201–210.
29. Groppi G, Belloli A, Tronconi E, Forzatti P. A comparison of lumped and distributed models of monolithic catalytic combustors. *Chem Eng Sci*. 1995;50:2705–2715.
30. Ramanathan K, West DH, Balakotaiah V. Optimal design of catalytic converters for minimizing cold-start emissions. *Catal Today*. 2004;98:357–373.
31. Ramanathan K, Balakotaiah V, West DH. Ignition criterion for general kinetics in a catalytic monolith. *AIChE J*. 2006;52:1623–1629.
32. Ramanathan K, Balakotaiah V, West DH. Light-off criterion and transient analysis of catalytic monoliths. *Chem Eng Sci*. 2003;58: 1381–1405.
33. Please CP, Hagan PS, Schwendeman DW. Light-off behavior of catalytic converters. *SIAM J Appl Math*. 1994;54:72–92.
34. Leighton DT, Chang H-C. A theory for fast-igniting catalytic converters. *AIChE J*. 1995;41:1898–1914.
35. Keith JM, Chang H-C, Leighton DT. Designing a fast-igniting catalytic converter system. *AIChE J*. 2001;47:650–663.
36. Todd B, Young JB. Thermodynamic and transport properties of gases for use in solid oxide fuel cell modeling. *J Power Sources*. 2002;110:186–200.
37. Fuller EN, Schettler PD, Giddings JC. A new method for prediction of binary gas-phase diffusion coefficients. *Ind Eng Chem*. 1966; 58:19–27.
38. Psyllos A, Philippopoulos C. Modelling of monolithic converters with axial catalyst distribution. *Appl Math Model*. 1993;17:459–467.
39. Baba N, Ohsawa K, Sugiura S. Numerical approach for improving the conversion characteristics of exhaust catalysts under warming-up condition. SAE Technical Paper Series. Paper No. 962076. 1996.
40. Kandylas IP, Stamatelos AM, Dimitriadis SG. Statistical uncertainty in automotive emissions testing. *Proc Instn Mech Eng Part D: J Automobile Eng*. 1999;213:491–502.
41. Kallinen K, Suopanki A, Härkönen M. Laboratory scale simulation of three-way catalyst engine ageing. *Catal Today*. 2005;100:223–228.
42. Holder R, Bollig M, Anderson DR, Hochmuth JK. A discussion on transport phenomena and three-way kinetics of monolithic converters. *Chem Eng Sci*. 2006;61:8010–8027.
43. Andersson J, Antonsson M, Eurenius L, Olsson E, Skoglundh M. Deactivation of diesel oxidation catalysts: vehicle- and synthetic aging correlations. *Appl Catal B: Environ*. 2007;72:71–81.
44. Fogler SH. *Elements of Chemical Reaction Engineering*, 3rd ed. NJ: Prentice Hall, 1998.
45. Froment GF, Bischoff KB. *Chemical Reactor Analysis and Design*, 2nd ed. New York: Wiley, 1990.
46. Kuo JCW, Morgan CR, Lassen HG. Mathematical modeling of CO and HC catalytic converter systems. SAE Technical Paper Series. Paper No. 710289. 1971.

Appendix

It is instructive to consider the special case of infinite solid conduction in the substrate walls, it is possible to arrive at some results to understand the light-off behavior under these limiting conditions. For infinite solid conductivity the wall temperature is essentially uniform along the monolith channel. So when light-off occurs in the monolith, it does so uniformly along the channel length and there is no specific light-off location. Using the assumptions listed earlier in developing the model for light-off analysis, the solid phase energy balance in this case can be written as

$$\frac{wC_{\mathrm{p,g}}}{A}\left(e^{\frac{hSAL}{wCp,g}}-1\right)(T_{\mathrm{g,in}}-T_{\mathrm{s}})-L\sum_{j=1}^{n\mathrm{Rct}}a_j(\Delta H)_j R_j(x_{\mathrm{g,in}},T_{\mathrm{s}})=0 \tag{A1}$$

where the length of the monolith channel appears explicitly in the balance equation. The light-off temperature for this special case is obtained by differentiating the above equation partially with respect to T_{s} and setting it equal to zero to get,

$$-hS\left[\frac{1}{B}(e^B-1)\right] -\sum_{j=1}^{n\mathrm{Rct}}a_j(\Delta H)_j\frac{d}{dT_{\mathrm{s}}}\left(R_j(x_{\mathrm{g,in}},T_{\mathrm{s}})\right)=0 \quad \text{where} \quad B=\frac{hSL}{wC_{\mathrm{p,g}}/A}. \tag{A2}$$

By virtue of the property that

$$\frac{1}{B}(e^B-1)>1 \text{ for all } B>0$$

and by comparing Eq. A2 with Eq. 9 we can conclude that the light-off temperature for the case of infinite solid conduction is always higher than that obtained for the case of finite solid conduction. This is because the heat generated by the reactions spread immediately (because of infinite solid conduction) and this heat loss has to be compensated for by a higher light-off temperature. Also, as mentioned earlier, there is no localized light-off and hence the time required for light-off would also be higher (see also section on the general transient analysis). Note that although the light-off temperature is higher and the light-off is delayed for the case of infinite solid conduction, once light-off has occurred the entire monolith channel is on the high temperature branch (and not in the kinetically controlled regime) and hence would have higher conversions compared to the case of finite solid conduction where only the $(L - z_{\mathrm{lo}})$ segment of the monolith is on the high temperature branch of the system.

Finally, as the length of the monolith channel is reduced, the light-off temperature approaches the value obtained for finite solid conduction as the light-off behavior gets forcibly localized. This is also evident from the fact that in the limit as $L\to 0$ (i.e. $B\to 0$) we have $\lim_{B\to 0}\frac{1}{B}(e^B-1)=1$ and Eq. A2 reduces to Eq. 9.

Manuscript received Nov. 20, 2007, and revision received Apr. 11, 2008.